20

Unified Power Flow Controllers

Ali Feliachi
West Virginia University

Azra Hasanovic
West Virginia University

Karl Schoder
West Virginia University

20.1 Introduction

An electric power system is an interconnection of generating units to load centers through high-voltage electric transmission lines. It consists of generation, transmission, and distribution subsystems, which used to belong to the same electric utility in a given geographical area. But, currently, the electric power industry is in transition from large, vertically integrated utilities providing power at regulated rates to an industry that will incorporate competitive companies selling unbundled power at possibly lower rates. With this new structure, which will include separate generation, distribution, and transmission companies with an open-access policy, comes the need for tighter control strategies. The strategies must maintain the level of reliability that consumers not only have taken for granted but expect even in the event of considerable structural changes, such as a loss of a large generating unit or a transmission line, and loading conditions, such as the continuous variations in power consumption. The deregulation of electricity that is taking place now will affect all business aspects of the power industry as known today from generation, to transmission, distribution, and consumption. Transmission circuits, in particular, will be stretched to their thermal limits because existing transmission lines are loaded close to their stability limits and building of new transmission circuits is difficult, if not impossible, at least from environmental and/or political aspects. New equipment and control devices will be sought to control power flow on transmission lines and to enhance stability and reliability of the system. Flexible AC transmission systems (FACTS) and FACTS controllers, which are power electronics devices used to control the power flow and enhance stability, have become common words in the power industry, and they have started replacing many mechanical control devices. They are certainly playing an increasingly major role in the operation and control of

today's power systems. This chapter describes specifically the Unified Power Flow Controller known as the UPFC. This power electronics device consists of two back-to-back converters operated from a common DC-link supplied by a capacitor. It is used to control the power flow between two nodes and also to enhance the stability of the system.

The chapter is organized as follows. First, a brief overview of the power flow on a transmission line is given. Second, the UPFC is described and its steady-state and basic operations are explained. Third, steady-state and dynamic models of the UPFC are presented. Also, a procedure to interface the UPFC with an electric power system is developed. Finally, supplementary signals through the UPFC, designed using fuzzy logic control tools, are shown to enhance the stability of the system by damping low-frequency oscillations. A two-area four-generator electric power system is used as a test system.

20.2 Power Flow on a Transmission Line

The power flow on a transmission line connecting two buses S and R (line sending and receiving buses) is briefly reviewed. The transmission line, as shown in Fig. 20.1, is modeled by a lumped series impedance, $Z = R + jX$, where R and X are the resistance and reactance of the line, respectively.

The complex power, S_S, leaving the sending bus and flowing toward the receiving bus is given by

$$S_S = \bar{V}_S \cdot \bar{I}^*_{\text{Line}} \tag{20.1}$$

where

$\bar{V}_S = V_S \angle \delta_S$ is the rms phasor voltage of the sending bus
$\bar{I}^*_{\text{Line}}$ = the complex conjugate of the phasor current on the line

The real and reactive powers are obtained from the complex power:

$$S_S = P_S + jQ_S \tag{20.2}$$

The line current, using Ohm's law, is

$$\bar{I}_{\text{Line}} = \frac{\bar{V}_S - \bar{V}_R}{Z} = (\bar{V}_S - \bar{V}_R)Y = (\bar{V}_S - \bar{V}_R)(G + jB) \tag{20.3}$$

where

$$Y = G + jB = \frac{1}{Z} = \frac{1}{R + jX} = \frac{R}{R^2 + X^2} - j\frac{X}{R^2 + X^2}$$

Therefore, the conductance and susceptance of the line are

$$G = \frac{R}{R^2 + X^2} = \frac{R}{X^2\left(1 + \left(\frac{R}{X}\right)^2\right)}$$

$$B = -\frac{X}{R^2 + X^2} = -\frac{\frac{1}{X}}{1 + \left(\frac{R}{X}\right)^2}$$

Hence, using Eqs. (20.1) and (20.3), the complex conjugate of the complex power is

$$S^*_S = P_S - jQ_S = \bar{V}^*_S \cdot \bar{I}_S = \bar{V}^*_S \cdot (\bar{V}_S - \bar{V}_R)(G + jB) = (V^2_S - \bar{V}^*_S \bar{V}_R)(G + jB) \tag{20.4}$$

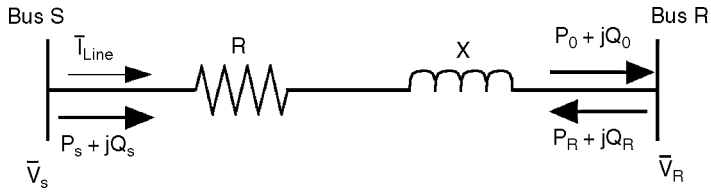

FIGURE 20.1 Transmission line.

Euler's identity, which states that $V\angle -\delta = V(\cos\delta - j\sin\delta)$, is used to write:

$$\bar{V}_S^* \bar{V}_R = (V_S \angle -\delta_S)(V_R \angle \delta_R) = V_S V_R \angle(-(\delta_S - \delta_R)) = V_S V_R(\cos(\delta_S - \delta_R) - j\sin(\delta_S - \delta_R)) \tag{20.5}$$

Substituting Eq. (20.5) into Eq. (20.4), the real and reactive powers are obtained:

$$P_S = V_S^2 G - V_S V_R G\cos(\delta_S - \delta_R) - V_S V_R B\sin(\delta_S - \delta_R) \tag{20.6}$$

$$Q_S = -V_S^2 B - V_S V_R G\sin(\delta_S - \delta_R) + V_S V_R B\cos(\delta_S - \delta_R) \tag{20.7}$$

Similarly, the real and reactive powers received at the receiving bus are

$$P_0 = -P_R = -V_R^2 G + V_S V_R G\cos(\delta_S - \delta_R) - V_S V_R B\sin(\delta_S - \delta_R) \tag{20.8}$$

$$Q_0 = -Q_R = V_R^2 B - V_S V_R G\sin(\delta_S - \delta_R) - V_S V_R B\cos(\delta_S - \delta_R) \tag{20.9}$$

In the above equations P_R and Q_R represent the powers leaving the receiving bus and flowing toward the sending bus. The power lost on the line is obtained by subtracting the power received from the power sent. Therefore, the real and reactive line losses are

$$P_L = P_S - (-P_R) = (V_S^2 + V_R^2)G - 2V_S V_R G\cos(\delta_S - \delta_R) \tag{20.10}$$

$$Q_L = Q_S - (-Q_R) = -(V_S^2 + V_R^2)B + 2V_S V_R B\cos(\delta_S - \delta_R) \tag{20.11}$$

For typical transmission lines the reactance X is a lot larger than the resistance R, i.e., the ratio R/X is very small and usually the conductance G is neglected and the susceptance B is approximated with $B = -1/X$. Using these approximations, Eqs. (20.6) and (20.8) yield the power transmitted over the line from the sending bus to the receiving bus:

$$P_S = -P_R = P_{SR} = -V_S V_R B\sin(\delta_S - \delta_R) = \frac{V_S V_R}{X}\sin(\delta_S - \delta_R) = \frac{V_S V_R}{X}\sin(\delta) = P_0(\delta) \tag{20.12}$$

where the angle $\delta = \delta_S - \delta_R$ is called the power angle.

The reactive power sent to the line from both buses is

$$Q_S = -V_S^2 B + V_S V_R B \cos(\delta_S - \delta_R) = \frac{V_S^2 - V_S V_R \cos(\delta)}{X} \tag{20.13}$$

$$Q_R = -V_R^2 B + V_S V_R B \cos(\delta_S - \delta_R) = \frac{V_R^2 - V_S V_R \cos(\delta)}{X} = -Q_0(\delta) \tag{20.14}$$

The average reactive power flow is defined as

$$Q_{SR} = \frac{Q_S - Q_R}{2} = -\frac{(V_S^2 - V_R^2)B}{2} = \frac{V_S^2 - V_R^2}{2X} \tag{20.15}$$

Equations (20.12) and (20.15) are the basis for understanding the control of power flow on a transmission line. From Eq. (20.12), it is seen that to increase the amount of real power transmitted over the line one can:

- Increase the magnitude of the voltages at either end, i.e., voltage support
- Reduce the reactance of the line, i.e., line compensation
- Increase the power angle, i.e., phase shift

One can also reverse the power flow by changing the sign of the power angle; i.e., a positive power angle will correspond to a power flow from sending to receiving, whereas a negative power angle $\delta_R > \delta_S$ will correspond to a power flow from receiving to sending.

Similarly, from Eq. (20.15), it is seen that both voltage magnitudes and line reactance will affect the reactive power. If both voltage magnitudes are the same, i.e., flat voltage profile, each bus will send half of the reactive power absorbed by the line. The power flow is from sending to receiving when $V_R < V_S$.

Hence, the four parameters that affect real and reactive power flows are V_S, V_R, X, and δ. To further understand this relationship, Eqs. (20.12) and (20.14) can be combined:

$$(P_0(\delta))^2 + \left(Q_0(\delta) + \frac{V_R^2}{X}\right)^2 = \left(\frac{V_S V_R}{X}\right)^2 \tag{20.16}$$

This equation represents a circle centered at $(0, -V_R^2/X)$, with a radius $V_S V_R/X$. It relates real and reactive powers received at bus R to the four parameters: V_S, V_R, δ, X. To see, for example, how the power angle δ affects P_0 and Q_0, assume that $V_S = V_R = V$ and $V^2/X = 1$. The P-Q locus for this case is shown in Fig. 20.2 (solid line). For a specific power angle δ, values of P_0 and Q_0 can be found, e.g., if $\delta = \pi/4$ (point A on the circle) then $P_{0A} = 0.707$ and $Q_{0A} = -0.293$. Reducing the line reactance X, say to $X' < X$, while keeping $V_S = V_R = V$, will increase the radius of the circle (dashed line). Note that the power angle δ might be constrained by stability limits.

Similarly, the relationship between the real and reactive powers sent to the line from the sending bus S can be expressed as

$$(P_S(\delta))^2 + \left(Q_S(\delta) - \frac{V_S^2}{X}\right)^2 = \left(\frac{V_S V_R}{X}\right)^2 \tag{20.17}$$

20.3 UPFC Description and Operation

The UPFC is one of the most complex FACTS devices in a power system today. It is primarily used for independent control of real and reactive power in transmission lines for a flexible, reliable, and economic operation and loading of power systems. Until recently all four parameters that affect real and reactive power flow on the line, i.e., line impedance, voltage magnitudes at the terminals of the line, and power angle, were controlled separately using either mechanical or other FACTS devices such as a static var

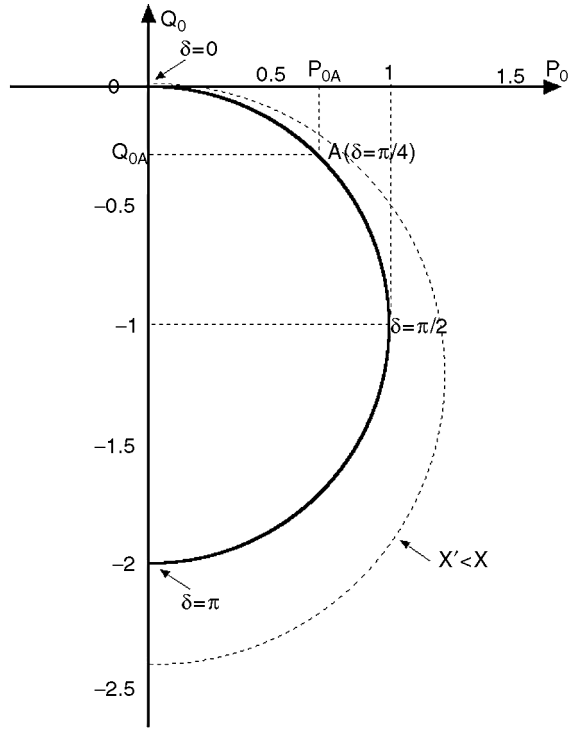

FIGURE 20.2 *P-Q* locus of the uncompensated system.

compensator (SVC), thyristor-controlled series compensation (TCSC), a phase shifter, etc. However, the UPFC allows simultaneous or independent control of all four parameters, with possible switching from one control scheme to another in real time. Also, the UPFC can be used for voltage support and transient stability improvement by damping of low-frequency power system oscillations.

The UPFC is a device placed between two buses referred to as the UPFC sending bus and the UPFC receiving bus. It consists of two voltage-sourced converters (VSCs) with a common DC-link. For the fundamental frequency model, the VSCs are replaced by two controlled voltage sources as shown in Fig. 20.3.

By applying the pulse width modulation (PWM) technique to the two VSCs, the following equations for magnitudes of shunt and series injected voltages can be obtained [2]:

$$V_{SH} = m_{SH}\frac{V_{DC}}{2\sqrt{2}n_{SH}V_B}$$
$$V_{SE} = m_{SE}\frac{V_{DC}}{2\sqrt{2}n_{SE}V_B} \tag{20.18}$$

where

m_{SH} = amplitude modulation index of the shunt VSC control signal
m_{SE} = amplitude modulation index of the series VSC control signal
n_{SH} = shunt transformer turn ratio
n_{SE} = series transformer turn ratio
V_B = the system side base voltage in kV
V_{DC} = DC-link voltage in kV

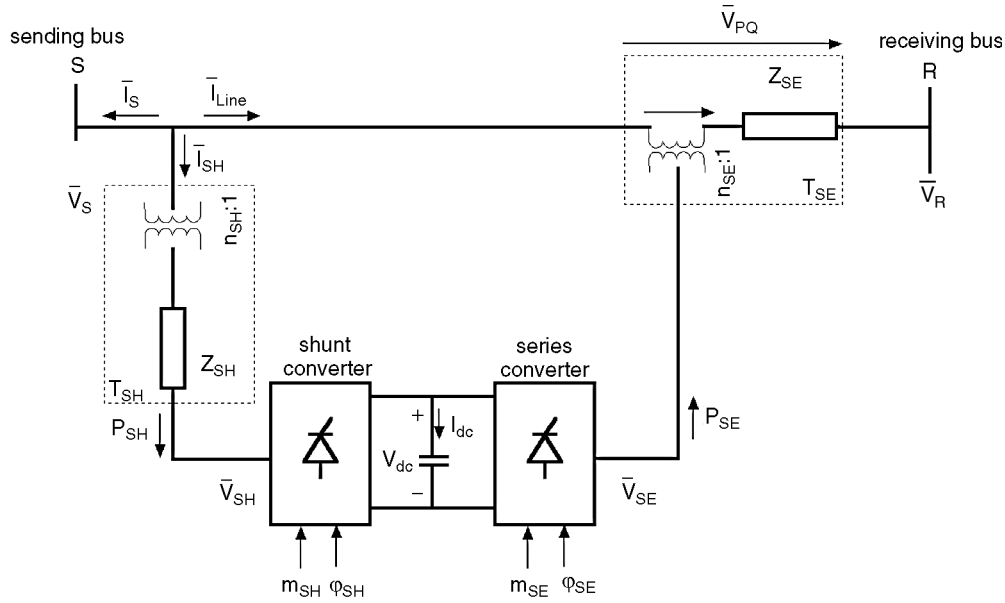

FIGURE 20.3 Fundamental frequency UPFC model.

The phase angles of $\bar{V}_{SH}$ and $\bar{V}_{SE}$ are

$$\begin{aligned} \delta_{SH} &= \delta_S - \varphi_{SH} \\ \delta_{SE} &= \delta_S - \varphi_{SE} \end{aligned} \tag{20.19}$$

where

φ_{SH} = firing angle of the shunt VSC with respect to the phase angle of the sending bus voltage
φ_{SE} = firing angle of the series VSC with respect to the phase angle of the sending bus voltage

The voltage source at the sending bus is connected in shunt and will therefore be called the *shunt voltage source*. The second source, the *series voltage source*, is placed between the sending and the receiving buses. Both voltage sources are modeled to inject voltages of fundamental power system frequency only. The UPFC is placed on high-voltage transmission lines. This arrangement requires step-down transformers to allow the use of power electronic devices for the UPFC. The transformer impedances have been included in the model.

The series converter injects an AC voltage $\bar{V}_{SE} = V_{SE} \angle(\delta_S - \varphi_{SE})$ in series with the transmission line. The series voltage magnitude V_{SE} and its phase angle φ_{SE} with respect to the sending bus are controllable in the range of $0 \le V_{SE} \le V_{SE\,max}$ and $0 \le \varphi_{SE} \le 360°$. The shunt converter injects controllable shunt voltage such that the real component of the current in the shunt branch balances the real power demanded by the series converter. The reactive power cannot flow through the DC-link. It is absorbed or generated (exchanged) locally by each converter. The shunt converter operated to exchange the reactive power with the AC system provides the possibility of independent shunt compensation for the line. If the shunt-injected voltage is regulated to produce a shunt reactive current component that will keep the sending bus voltage at its prespecified value, then the shunt converter is operated in the *automatic voltage control mode*. The shunt converter can also be operated in the *VAr control mode*. In this case, shunt reactive current is produced to meet the desired inductive or capacitive VAr request.

Series Converter: Four Modes of Operation

As mentioned previously, the UPFC can control, independently or simultaneously, all parameters that affect power flow on a transmission line. This is illustrated in the phasor diagrams shown in Fig. 20.4 [3].

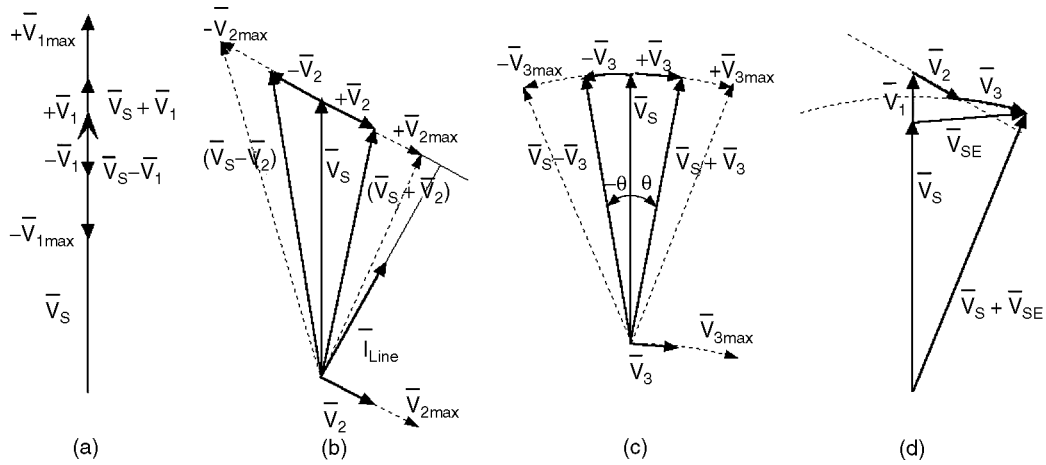

FIGURE 20.4 Phasor diagrams.

Voltage regulation is shown in Fig. 20.4a. The magnitude of the sending bus voltage $\bar{V}_S$ is increased (or decreased) by injecting a voltage $\bar{V}_1$, of maximum magnitude V_{1max}, in phase (or out of phase) with $\bar{V}_S$. Similar regulation can be accomplished with a transformer tap changer.

Series reactive compensation is shown in Fig. 20.4b. It is obtained by injecting a voltage $\bar{V}_2$, of maximum magnitude V_{2max}, orthogonal to the line current $\bar{I}_{Line}$. The effective voltage drop across the line impedance X is decreased (or increased) if the voltage $\bar{V}_2$ lags the current $\bar{I}_{Line}$ by 90° (or $\bar{V}_2$ leads current $\bar{I}_{Line}$ by 90°).

A desired phase shift is achieved by injecting a voltage $\bar{V}_3$, of maximum magnitude V_{3max}, that shifts the phase angle of $\bar{V}_S$ by $\pm\theta$ while keeping its magnitude constant as shown in Fig. 20.4c.

Simultaneous control of terminal voltage, line impedance, and phase angle allows the UPFC to perform multifunctional power flow control. The magnitude and the phase angle of the series injected voltage $\bar{V}_{SE} = \bar{V}_1 + \bar{V}_2 + \bar{V}_3$, shown in Fig. 20.4d, are selected in a way to produce a line current that will result in the desired real and reactive power flow on the transmission line.

Therefore, the UPFC series converter can be operated in any of the following four modes:

1. Voltage regulation
2. Line compensation
3. Phase angle regulation
4. Power flow control

Automatic Power Control

The automatic power control mode cannot be accomplished with conventional compensators. To show how line power flow can be affected by the UPFC operated in the automatic power flow control mode, a UPFC is placed at the beginning of the transmission line connecting buses S and R as shown in Fig. 20.5 [3]. Line conductance is neglected. UPFC is represented by two ideal voltage sources of controllable magnitude and phase angle. Bus S and fictitious bus S_1 shown in Fig. 20.5 represent the UPFC sending and receiving buses, respectively.

In this case, the complex power received at the receiving end of the line is given by

$$S = \bar{V}_R \bar{I}^*_{Line} = \bar{V}_R \left(\frac{\bar{V}_S + \bar{V}_{SE} - \bar{V}_R}{jX} \right)^* \tag{20.20}$$

where $\bar{V}_{SE} = V_{SE} \angle (\delta_S - \varphi_{SE})$.

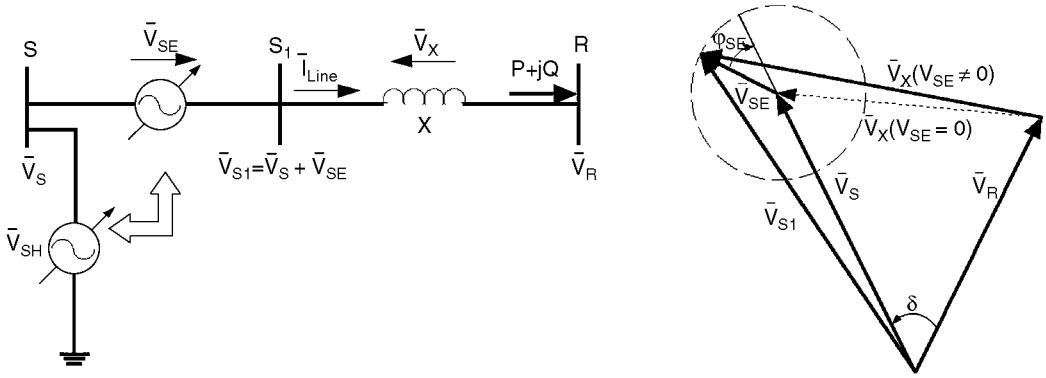

FIGURE 20.5 Transmission line with UPFC.

The complex conjugate of this complex power is

$$S^* = P - jQ = \bar{V}_R^*\left(\frac{\bar{V}_S + \bar{V}_{SE} - \bar{V}_R}{jX}\right) \tag{20.21}$$

By performing simple mathematical manipulations and separating real and imaginary parts of Eq. (20.21), the following expressions for real and reactive powers received at the receiving end of the line are

$$\begin{aligned} P &= \frac{V_S V_R}{X}\sin\delta + \frac{V_R V_{SE}}{X}\sin(\delta - \varphi_{SE}) = P_0(\delta) + P_{SE}(\delta, \varphi_{SE}) \\ Q &= -\frac{V_R^2}{X} + \frac{V_S V_R}{X}\cos\delta + \frac{V_R V_{SE}}{X}\cos(\delta - \varphi_{SE}) = Q_0(\delta) + Q_{SE}(\delta, \varphi_{SE}) \end{aligned} \tag{20.22}$$

For $V_{SE} = 0$ the above equations are identical to Eqs. (20.12) and (20.14) that represent the real and reactive powers of the uncompensated system.

It was stated previously that the UPFC series voltage magnitude can be controlled between 0 and $V_{SE\,max}$ and its phase angle can be controlled between 0 and 360° at any power angle δ. It can be seen from Eq. (20.21) that the real and reactive power received at bus R for the system, when a UPFC is installed, can be controlled between

$$\begin{aligned} P_{min}(\delta) \le P \le P_{max}(\delta) \\ Q_{min}(\delta) \le Q \le Q_{max}(\delta) \end{aligned} \tag{20.23}$$

where

$$\begin{aligned} P_{min}(\delta) &= P_0(\delta) - \frac{V_R V_{SEmax}}{X} \\ P_{max}(\delta) &= P_0(\delta) + \frac{V_R V_{SEmax}}{X} \\ Q_{min}(\delta) &= Q_0(\delta) - \frac{V_R V_{SEmax}}{X} \\ Q_{max}(\delta) &= Q_0(\delta) + \frac{V_R V_{SEmax}}{X} \end{aligned}$$

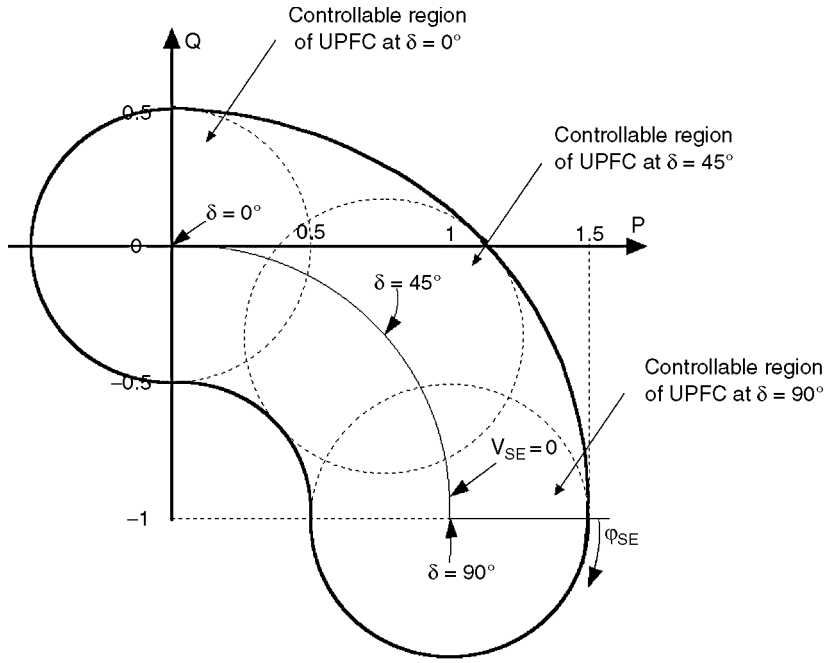

FIGURE 20.6 *P-Q* relationship for a simple two-bus system with a UPFC at $\delta = 0°$, 45°, and 90°.

Rotation of the series injected voltage phasor with rms value of $V_{SE\,max}$ from 0 to 360° allows the real and the reactive power flow to be controlled within the boundary circle with a radius of $V_R V_{SE\,max}/X$ and the center at $(P_0(\delta), Q_0(\delta))$. This circle is defined by the following equation:

$$(P(\delta, \varphi_{SE}) - P_0(\delta))^2 + (Q(\delta, \varphi_{SE}) - Q_0(\delta))^2 = \left(\frac{V_R V_{SE\,max}}{X}\right)^2 \tag{20.24}$$

Figure 20.6 shows plots of the reactive power Q demanded at the receiving bus vs. the transmitted real power P as a function of the series voltage magnitude V_{SE} and phase angle φ_{SE} at three different power angles δ, i.e., $\delta = 0°$, 45°, and 90°, with $V_S = V_R = V$, $V^2/X = 1$ and $V_R V_{SE\,max}/X = 0.5$ [3]. The capability of the UPFC to control real and reactive power flow independently at any transmission angle is clearly illustrated in Fig. 20.6.

20.4 UPFC Modeling

To simulate a power system that contains a UPFC, the UPFC needs to be modeled for steady-state and dynamic operations. Also, the UPFC model needs to be interfaced with the power system model. Hence, in this section modeling and interfacing of the UPFC with the power network are described.

UPFC Steady-State or Load Flow Model

For steady-state operation the DC-link voltage remains constant at its prespecified value. In the case of a lossless DC-link the real power supplied to the shunt converter $P_{SH} = \mathrm{Re}(\bar{V}_{SH}\bar{I}^*_{SH})$ satisfies the real power demanded by the series converter $P_{SH} = \mathrm{Re}(\bar{V}_{SE}\bar{I}^*_{Line})$

$$P_{SH} = P_{SE} \tag{20.25}$$

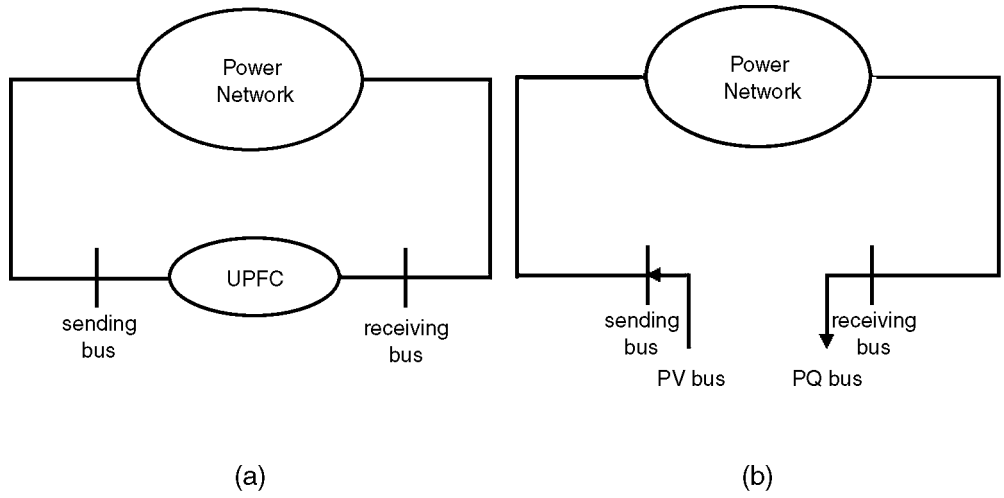

FIGURE 20.7 Power network with a UPFC included: (a) schematic; (b) LF model.

The LF model discussed here assumes that the UPFC is operated to keep (1) real and reactive power flows at the receiving bus and (2) sending bus voltage magnitude at their prespecified values [4]. In this case, the UPFC can be replaced by an "equivalent generator" at the sending bus (PV-type bus using LF terminology) and a "load" at the receiving bus (*PQ*-type bus) as shown in Fig. 20.7.

To obtain the LF solution of a power network that contains a UPFC, an iterative procedure is needed. Power demanded at the receiving bus is set to the desired real and reactive powers at that bus. The real power injected into a PV bus for a conventional LF algorithm is kept constant and the reactive power is adjusted to achieve the prespecified voltage magnitude. With a UPFC, the real power injected into the sending bus is not known exactly. This real power injection is initialized to the value that equals the prespecified real power flow at the receiving bus. During the iterative procedure, the real powers adjusted to cover the losses of the shunt and series impedances and to force the sum of converter interaction to become zero. The algorithm, in its graphical form, is given in Fig. 20.8.

The necessary computations are described next. The complex power injected into sending bus is

$$\bar{S}_S = \bar{V}_S \bar{I}_S^* \tag{20.26}$$

Using the voltages and currents described in Fig. 20.3

$$\begin{aligned} \bar{V}_S &= \bar{V}_{\text{SH}} + \bar{V}_{Z_{\text{SH}}} \\ \bar{V}_{Z\text{SH}} &= \bar{I}_{\text{SH}} Z_{\text{SH}} \\ \bar{I}_S &= -\bar{I}_{\text{SH}} - \bar{I}_{\text{Line}} \end{aligned} \tag{20.27}$$

results in

$$\begin{aligned} S_S &= (\bar{V}_{\text{SH}} + \bar{V}_{Z_{\text{SH}}})(-\bar{I}_{\text{SH}} - \bar{I}_{\text{Line}})^* \\ &= -\bar{V}_{\text{SH}} \bar{I}_{\text{SH}}^* - \bar{V}_{Z\text{SH}} \bar{I}_{\text{SH}}^* - \bar{V}_{\text{SH}} \bar{I}_{\text{Line}}^* - \bar{V}_{Z_{\text{SH}}} \bar{I}_{\text{Line}}^* \\ &= -\bar{V}_{\text{SH}} \bar{I}_{\text{SH}}^* - Z_{\text{SH}} I_{\text{SH}}^2 - \bar{V}_{\text{SH}} \bar{I}_{\text{Line}}^* - Z_{\text{SH}} \bar{I}_{\text{SH}} \bar{I}_{\text{Line}}^* \end{aligned} \tag{20.28}$$

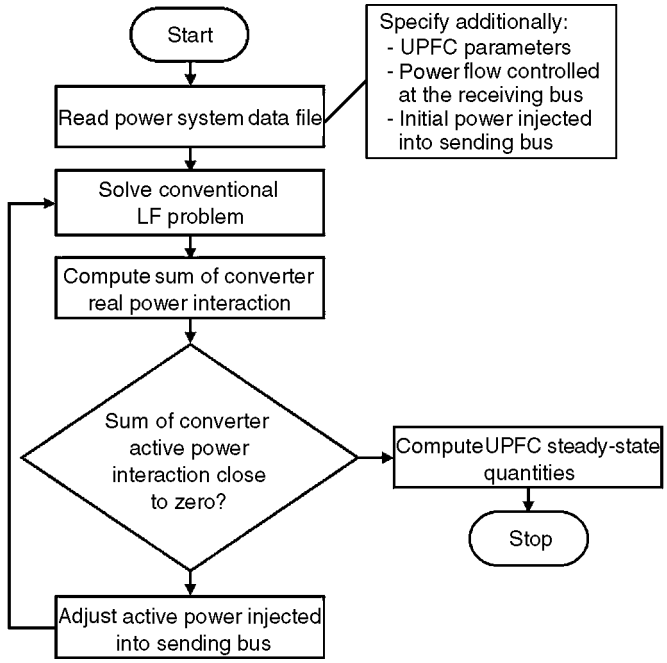

FIGURE 20.8 LF algorithm.

Computing the line current by using the bus voltages and the power flow at the receiving bus as given by the LF solution

$$\bar{I}_{\text{Line}} = -\frac{S_R^*}{\bar{V}_R^*} \tag{20.29}$$

allows one to compute the series injected voltage and the series converter interaction with the power system:

$$\begin{aligned} \bar{V}_{\text{SE}} &= \bar{I}_{\text{Line}} Z_{\text{SE}} + \bar{V}_R - \bar{V}_S \\ P_{\text{SE}} &= \text{Re}(\bar{V}_{\text{SE}} \bar{I}_{\text{Line}}^*) \end{aligned} \tag{20.30}$$

Taking the real part of Eq. (20.28) and using Eq. (20.25), the new injected real power at the sending bus becomes

$$P_S = -P_{\text{SE}} + \text{Re}\,(-Z_{\text{SH}} I_{\text{SH}}^2 - \bar{V}_{\text{SH}} \bar{I}_{\text{Line}}^* - Z_{\text{SH}} \bar{I}_{\text{SH}} \bar{I}_{\text{Line}}^*) \tag{20.31}$$

It should be noted that there is no need for an iterative procedure used in Ref. 4 to compute UPFC control parameters. They can be computed directly after a conventional LF solution satisfying Eq. (20.25) is found. By neglecting transformer losses and initializing the real power injected into the sending bus to the real power flow controlled on the line, the convergence of the proposed LF algorithm is obtained within one step.

UPFC Dynamic Model

For transient stability studies, the DC-link dynamics have to be taken into account and Eq. (20.25) can no longer be applied. The DC-link capacitor will exchange energy with the system and its voltage will vary.

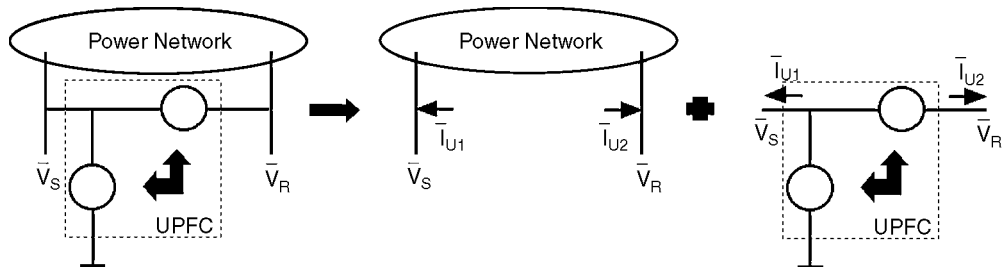

FIGURE 20.9 Interface of the UPFC with power network.

The power frequency dynamic model as given in Refs. 5 and 7 can be described by the following equation:

$$\mathrm{CV}_{\mathrm{DC}} \frac{dV_{\mathrm{DC}}}{dt} = (P_{\mathrm{SH}} - P_{\mathrm{SE}})S_B \tag{20.32}$$

Note that in the above equation the DC variables are expressed in MKSA units, whereas the AC system variables are expressed as per-unit quantities. S_B is the system side base power.

Interfacing the UPFC with the Power Network

The interface of the UPFC with the power network is shown in Fig. 20.9 [7].

To obtain the network solution (bus voltages and currents), an iterative approach is used. The UPFC sending and receiving bus voltages $\bar{V}_S$ and $\bar{V}_R$ can be expressed as a function of generator internal voltages $\bar{E}_G$ and the UPFC injection voltages $\bar{V}_{\mathrm{SH}}$ and $\bar{V}_{\mathrm{SE}}$ (Eq. 20.39). Control output and Eq. (20.18) determine the UPFC injection voltage magnitudes V_{SH} and V_{SE}. However, the phase angles of the injected voltages, δ_{SH} and δ_{SE}, are unknown because they depend on the phase angle of the sending bus voltage, δ_S, which is the result of the network solution. Graphical form of the algorithm for interfacing the UPFC with the power network is shown in Fig. 20.10. Necessary computations are shown below.

Reducing the bus admittance matrix to generator internal buses and UPFC terminal buses the following equation can be written

$$\begin{bmatrix} Y_{GG} & Y_{GU} \\ Y_{UG} & Y_{UU} \end{bmatrix} \begin{bmatrix} \bar{E}_G \\ \bar{V}_U \end{bmatrix} = \begin{bmatrix} \bar{I}_G \\ \bar{I}_U \end{bmatrix} \tag{20.33}$$

where

Y_{GG} = reduced admittance matrix connecting generator currents injection to the internal generator-voltages
Y_{GU} = admittance matrix component, which gives the generator currents due to the voltages at UPFC buses
Y_{UG} = admittance matrix component, which gives UPFC currents in terms of the generator internal voltages
Y_{UU} = admittance matrix connecting UPFC currents to the voltages at UPFC buses
$\bar{E}_G$ = vector of generator internal bus voltages
$\bar{V}_U$ = vector of UPFC AC bus voltages
$\bar{I}_G$ = vector of generator current injections
$\bar{I}_U$ = vector of UPFC currents injected to the power network

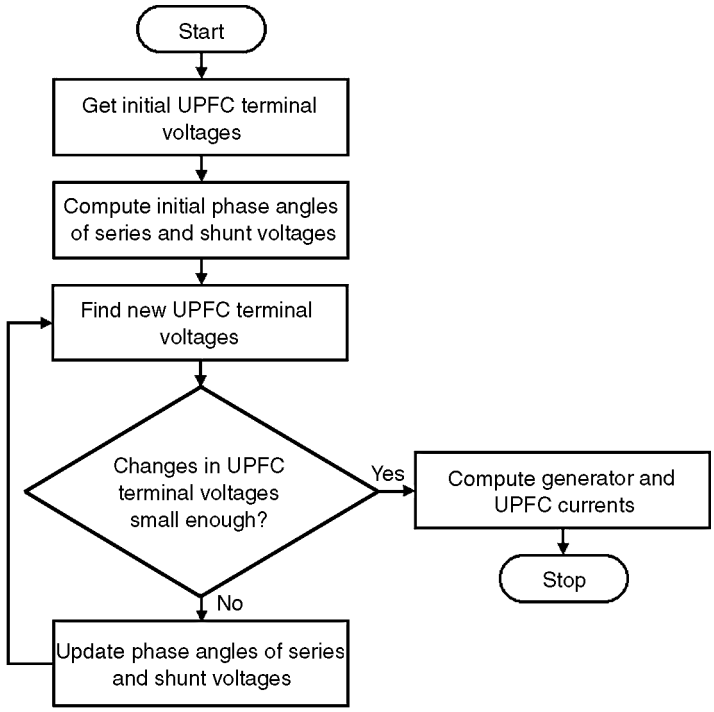

FIGURE 20.10 Algorithm for interfacing the UPFC with the power network.

The second equation of (20.33) is of the form

$$\bar{I}_U = Y_{UG}\bar{E}_G + Y_{UU}\bar{V}_U \tag{20.34}$$

By neglecting series and shunt transformer resistances, the following equations can be written for the UPFC currents injected into the power network (see Figs. 20.3 and 20.9):

$$\begin{aligned} \bar{I}_{U1} &= -\bar{I}_{\text{SH}} - \bar{I}_{\text{Line}} \\ \bar{I}_{U2} &= \bar{I}_{\text{Line}} \end{aligned} \tag{20.35}$$

$$\bar{I}_{\text{SH}} = \frac{\bar{V}_S - \bar{V}_{\text{SH}}}{jx_{\text{SH}}} \tag{20.36}$$

$$\bar{I}_{\text{Line}} = \frac{\bar{V}_{\text{SE}} + \bar{V}_S - \bar{V}_R}{jx_{\text{SE}}} \tag{20.37}$$

Combining the above equations yields the following equation:

$$\bar{I}_U = W_U\bar{V}_U + W_C\bar{V}_C \tag{20.38}$$

where

$$W_C = \begin{bmatrix} \dfrac{1}{jx_{\text{SH}}} & -\dfrac{1}{jx_{\text{SE}}} \\ 0 & \dfrac{1}{jx_{\text{SE}}} \end{bmatrix}$$

$$W_U = \begin{bmatrix} -\frac{1}{jx_{SE}} - \frac{1}{jx_{SH}} & \frac{1}{jx_{SE}} \\ \frac{1}{jx_{SE}} & -\frac{1}{jx_{SE}} \end{bmatrix}$$

$$\bar{I}_U = \begin{bmatrix} \bar{I}_{U1} \\ \bar{I}_{U2} \end{bmatrix}$$

$$\bar{V}_U = \begin{bmatrix} \bar{V}_S \\ \bar{V}_R \end{bmatrix}$$

$$\bar{V}_C = \begin{bmatrix} \bar{V}_{SH} \\ \bar{V}_{SE} \end{bmatrix}$$

By equating (20.34) with (20.38), the following equation for computation of UPFC terminal voltages can be written:

$$\bar{V}_U = (W_U - Y_{UU})^{-1} Y_{UG} \bar{E}_G - (W_U - Y_{UU})^{-1} W_C V_C = L_G \bar{E}_G + L_C \bar{V}_C \tag{20.39}$$

20.5 Control Design

To operate the UPFC in the automatic control mode discussed in the previous section, and also to use the UPFC to enhance power system stability and dampen low-frequency oscillations, two control designs need to be performed. A primary control design, referred to as the *UPFC basic control design*, involves simultaneous regulation of (1) real and reactive power flows on the transmission line, (2) sending bus voltage magnitude, and (3) DC voltage magnitude. A secondary control design, referred to as the *damping controller design*, is a supplementary control loop that is designed to improve transient stability of the entire electric power system. The two control designs are described in this section.

UPFC Basic Control Design

The UPFC basic control design consists of four separate control loops grouped into a *series control scheme*, whose objective is to maintain both real and reactive power flows on the transmission lines close to some prespecified values, and a *shunt control scheme*, whose objective is to control the sending bus voltage magnitude as well as the DC voltage magnitude.

Series Control Scheme

This scheme has two control loops, one for the tracking of the real power flow at the receiving bus of the line, and the second performing the same task for the reactive power flow. Specifically, the objective is to track these real and reactive power flows following step changes and to eliminate steady-state tracking errors. This is obtained by the appropriate selection of the voltage drop between the sending and the receiving buses, which is denoted $\bar{V}_{PQ}$. This voltage can be decomposed into the following two quantities, which affect the tracked powers, namely:

1. V_P = voltage component orthogonal to the sending bus voltage (it affects primarily the real power flow on the transmission line)
2. V_Q = component in phase with the sending bus voltage (it affects mainly the reactive power flow on the transmission line)

These quantities are in phasor diagram in Fig. 20.11.

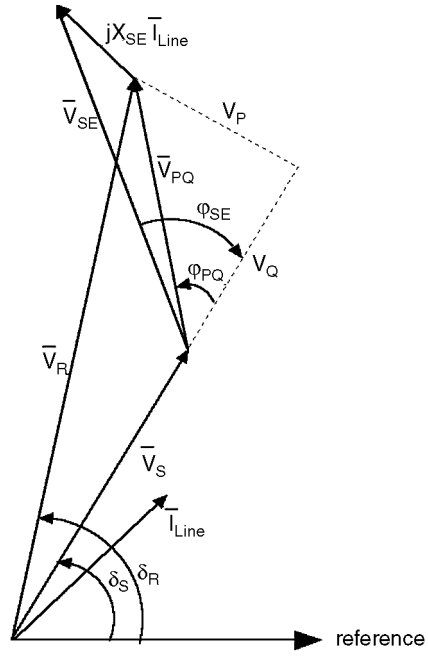

FIGURE 20.11 Phasor diagram.

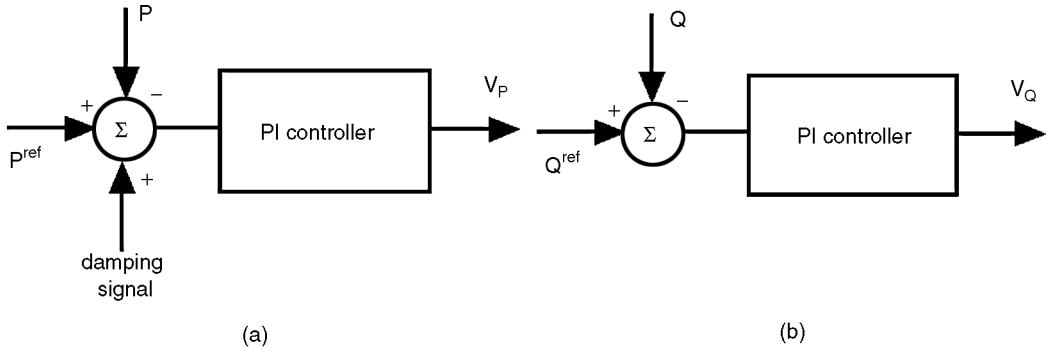

FIGURE 20.12 Series control scheme–automatic power flow mode.

Both voltages V_P and V_Q are obtained by designing classic PI (proportional-integral) controllers, as illustrated in Fig. 20.12 [7]. The integral controller will guarantee error-free steady-state control of the real and reactive line power flows.

After the V_P and V_Q components have been found, the series injected voltage are computed:

$$\begin{aligned} V_{PQ} &= \sqrt{V_P^2 + V_Q^2} \\ \varphi_{PQ} &= tg^{-1}\frac{V_P}{V_Q} \\ \bar{V}_{PQ} &= V_{PQ}\angle(\delta_S + \varphi_{PQ}) \\ \bar{V}_{SE} &= \bar{V}_{PQ} + jX_{SE}\bar{I}_{Line} \end{aligned} \tag{20.40}$$

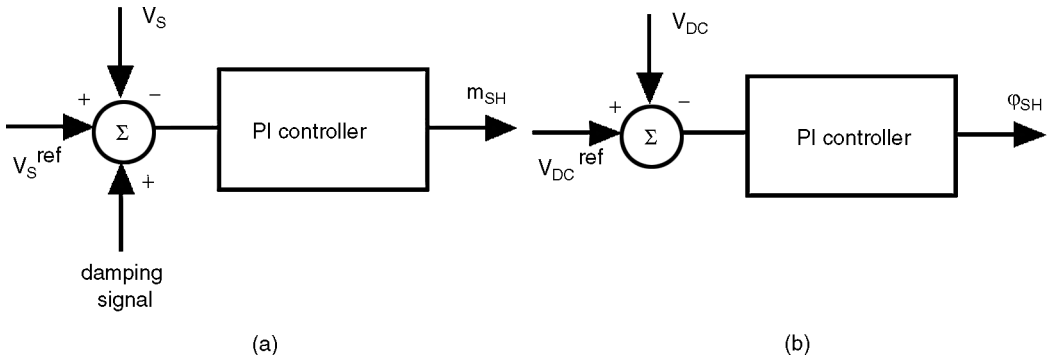

FIGURE 20.13 Shunt control scheme.

From Eqs. (20.18) and (20.19), series converter amplitude modulation index and firing angle are

$$m_{SE} = \frac{2\sqrt{2}n_{SE}V_{SE}V_B}{V_{DC}}$$
$$\varphi_{SE} = \delta_S - \delta_{SE} \tag{20.41}$$

Shunt Control Scheme

This control scheme also has two loops that are designed to maintain the magnitude of the sending bus voltage and the DC-link voltage at their prespecified values. The magnitude of the injected shunt voltage (Eq. 20.18) affects the reactive power flow in the shunt branch, which in turn affects the sending bus voltage magnitude. The angle between the sending bus voltage and the injected shunt voltage, φ_{SH} (Eq. 20.19), affects the real power flow in the shunt branch. It can be used to control the power flow to the DC-link and therefore the DC-link voltage. This is achieved by using two separate PI controllers as shown in Fig. 20.13 [6, 7].

Power System Damping Control through UPFC Using Fuzzy Control

Low-frequency oscillations in electric power systems occur frequently because of disturbances, such as changes in loading conditions or a loss of a transmission line or a generating unit. These oscillations need to be controlled to maintain system stability. Several control devices, such as power system stabilizers, are used to enhance power system stability. Recently [6–8], it has been shown that the UPFC can also be used to effectively control these low-frequency power system oscillations. It is done by designing a supplementary signal based on either the real power flow along the transmission line to the series converter side (Fig. 20.12a) or to the shunt converter side through the modulation of the voltage magnitude reference signal (Fig. 20.13a). The damping controllers used are of lead-lag type with transfer functions similar to the one shown in Fig. 20.14.

The authors of this chapter have designed a damping controller using fuzzy logic. This control design is presented here. But first, a brief review of fuzzy set theory and the basics of fuzzy control design is given.

Fuzzy Control Overview

Fuzzy control is based on fuzzy logic theory, but there is no systematic design procedure in fuzzy control. The important advantage of fuzzy control design is that a mathematical model of the system is not required.

Fuzzy controllers are rule-based controllers. The rules are given in the "if–then" format. The "if-side" is called condition and the "then-side" is called conclusion. The rules may use several variables both in condition and conclusion of the rules. Therefore, the fuzzy controllers can be applied to nonlinear

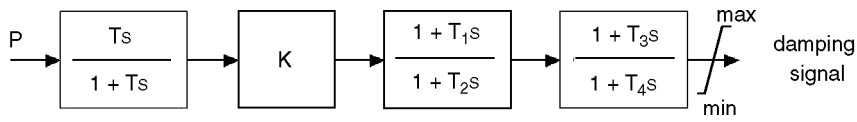

FIGURE 20.14 Lead–lag controller structure.

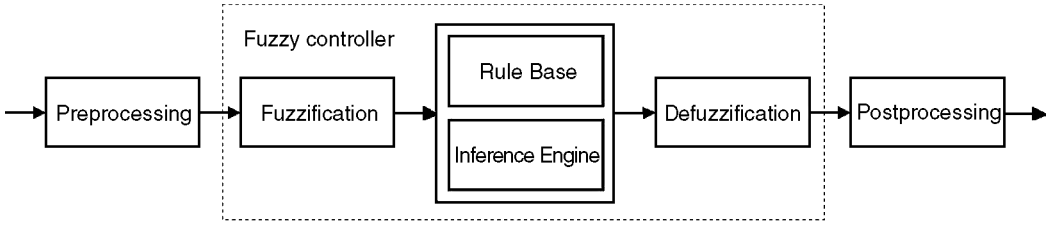

FIGURE 20.15 Fuzzy controller structure.

multiinput–multioutput (MIMO) systems such as power systems. The control rules can be found based on:

- Expert experience and control engineering knowledge of the system
- Learning (e.g., neural networks)

Fuzzy logic has its own terminology, which is reviewed below [10].

Fuzzy set: Let X be a collection of objects, then a fuzzy set A in X is defined as

$$A = \{(x, \mu_A(x)) | x \in X\} \tag{20.42}$$

$\mu_A(x)$ is called the membership function of x in A. It usually takes values in the interval [0, 1]. The numerical interval X relevant for the description of a fuzzy variable is called Universe of Discourse.

Operations on fuzzy sets: Let A and B be two fuzzy sets with membership functions $\mu_A(x)$ and $\mu_B(x)$. The *AND operator or intersection of two fuzzy sets* A and B is a fuzzy set C whose membership function $\mu_C(x)$ is defined as

$$\mu_C(x) = \min\{\mu_A(x), \mu_B(x)\}, \quad x \in X \tag{20.43}$$

The *OR operator or union of two fuzzy sets* A and B is a fuzzy set C whose membership function $\mu_C(x)$ is defined as

$$\mu_C(x) = \max\{\mu_A(x), \mu_B(x)\}, \quad x \in X \tag{20.44}$$

Next, the structure of a fuzzy controller is presented. A fuzzy controller structure is shown in Fig. 20.15 [9]. The controller is placed between preprocessing and post-processing blocks.

The *preprocessing block* conditions the inputs, crisp measurements, before they enter the controller.
First step in fuzzy controller design is to choose appropriate input and output signals of the controller.
Second step is to choose linguistic variables that will describe all input and output variables.
Third step is to define membership functions for fuzzy sets. Membership functions can be of different shape, i.e., triangular, trapezoidal, Gaussian functions, etc.

Fourth step is to define fuzzy rules. For two-input one-output system each control rule R_i will be of the following form:

$$\text{IF input (1) is } A_{i1} \text{ AND input (2) is } A_{i2} \text{ THEN output is } B_i$$

Fifth step is to join rules by using an inference engine. The most often used inference engines are *Mamdani Max–Min and Max-Product*. The Max-Product inference procedure can be summarized as

- For the *i*th rule
  - —Obtain the minimum between the input membership functions by using the AND operator
  - —Re-scale the output membership function by the obtained minimum to obtain the output membership function due to the *i*th rule
- Repeat the same procedure for all rules.
- Find the maximum between output membership functions obtained from each rule by using the OR operator. This gives the final output membership function due to all rules.

Graphical technique of Mamdani (Max-Product) inference is shown in Fig. 20.16. Graphical technique of Mamdani Max-Min inference shown in Fig. 20.17 can be explained in similar matter.

Sixth step is defuzzification. The resulting fuzzy set must be converted to a number. This operation is called defuzzification. The most often used defuzzification method is the centroid method or center of area as shown in Fig. 20.18.

Post-processing. The post-processing block often contains an output gain that can be tuned.

Fuzzy Logic UPFC Damping Controller

Input signals to the controller, power flow deviation ΔP and energy deviation ΔE, are derived from the real power flow signal at the UPFC site [11]. The signals, representing the accelerating power and energy of generators at both ends of the tie line, indicate a required change in transmitted line power flow and have to be driven back to zero for a new steady state by the damping controller. The process of finding these signals requires some signal conditioning as shown in Fig. 20.19. Filters are used to remove noise and offset components [11, 12].

The inputs are described by the following linguistic variables: P (positive), NZ (near zero), and N (negative). The output is described with five linguistic variables P (positive), PS (positive small), NZ (near zero), NS (negative small), and N (negative). Gaussian functions are used as membership functions for

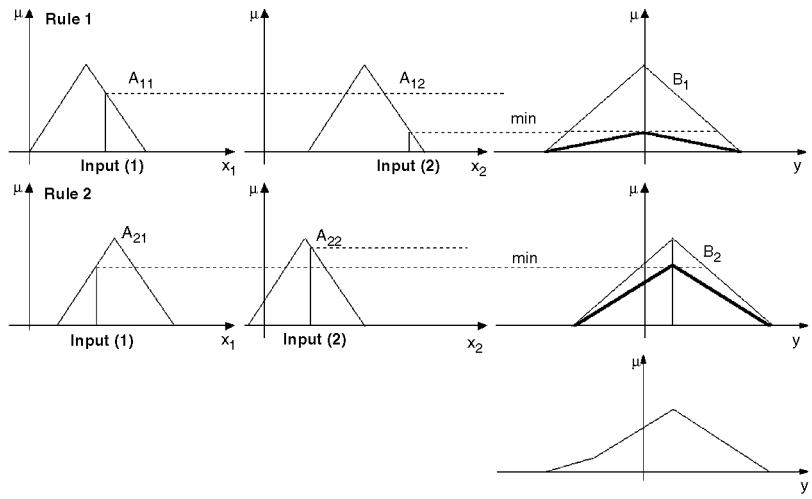

FIGURE 20.16 Mamdani Max-Product inference.

TABLE 20.1 Fuzzy Rules

if ΔE is NZ, then damping signal is NZ
if ΔE is P, then damping signal is P
if ΔE is N, then damping signal is N
if ΔE is NZ, and ΔP is P, then damping signal is NS
if ΔE is NZ, and ΔP is N, then damping signal is PS

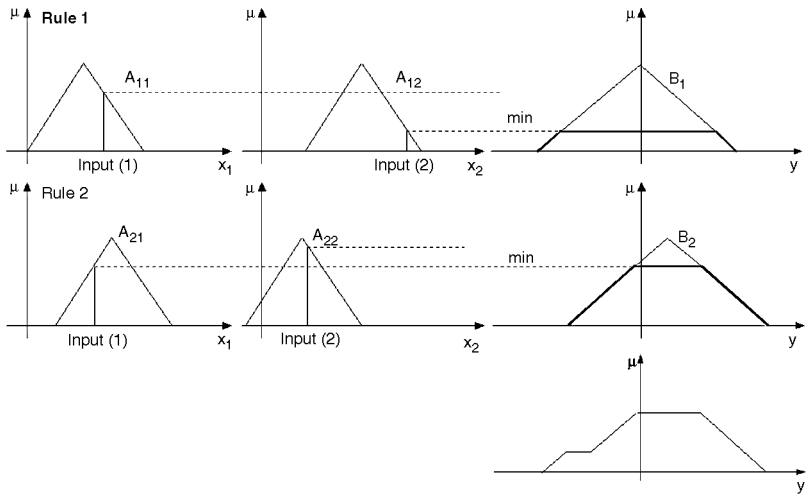

FIGURE 20.17 Mamdani (Max-Min) inference.

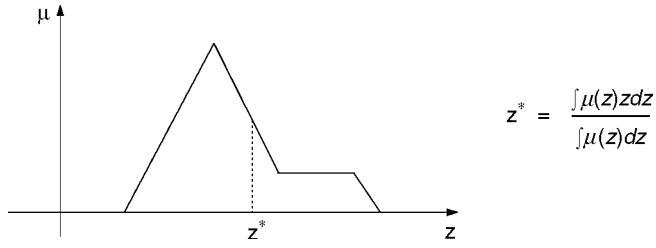

FIGURE 20.18 Centroid method.

FIGURE 20.19 Obtaining the input signals for fuzzy controller.

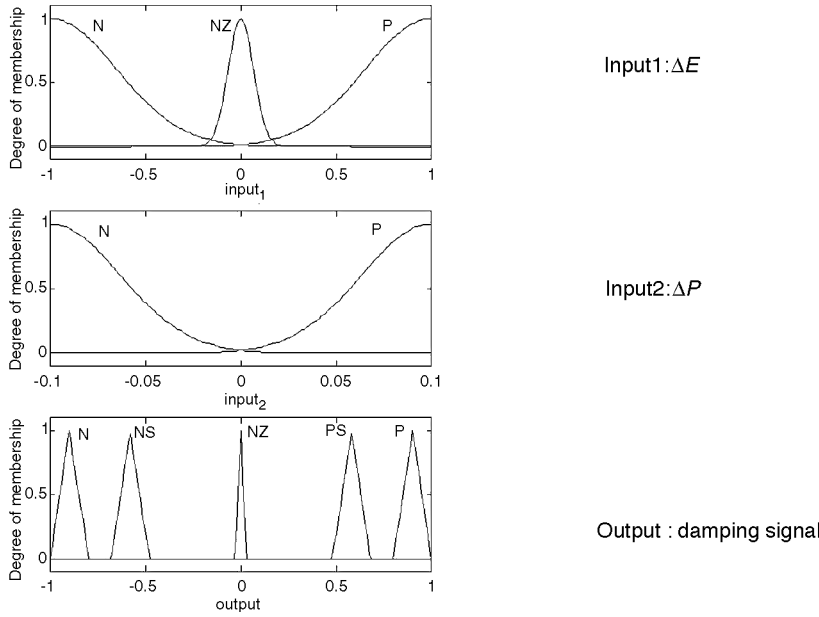

FIGURE 20.20 Fuzzy logic controller input and output variables.

both inputs, and triangular membership functions are used for output (Fig. 20.20). The damping signal is controller output. Fuzzy rules used are given in Table 20.1.

20.6 Case Study

Test System

The performance of the UPFC is tested on a two-area–four-generator system (test system) as shown in Figure 20.21. Data for this system can be found in Ref. 1.

The two areas are identical to one another and interconnected with two parallel 230-km tie lines that carry about 400 MW from area 1 (generators 1 and 2) to area 2 (generators 3 and 4) during normal operating conditions. The UPFC is placed at the beginning of the lower parallel line between buses 101 and 13 to control the power flow through that line as well as to regulate voltage level at bus 101. Two cases are considered:

1. UPFC performance when the real and reactive power references are changed
2. UPFC performance when a fault is applied

All simulations are carried out in the Power System Toolbox (PST) [1], a commercial MATLAB-based package for nonlinear simulation of power systems that was modified by the authors to include a UPFC model.

Tracking Real and Reactive Power Flows

The objective is to keep the sending bus voltage at its prespecified value and to:

- Keep the reactive power constant while tracking the step changes in the real power (UPFC is initially operated to control the real power flow at 1.6 pu; at time 0.5 s real power flow reference

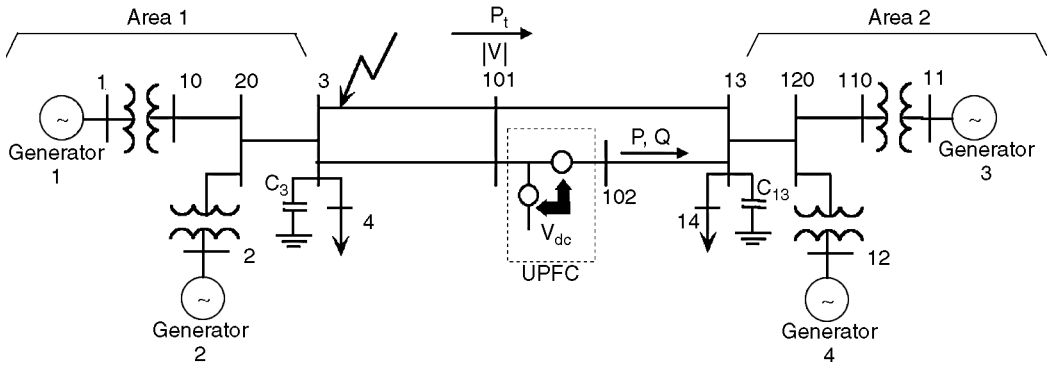

FIGURE 20.21 Two-area–four-generator test system.

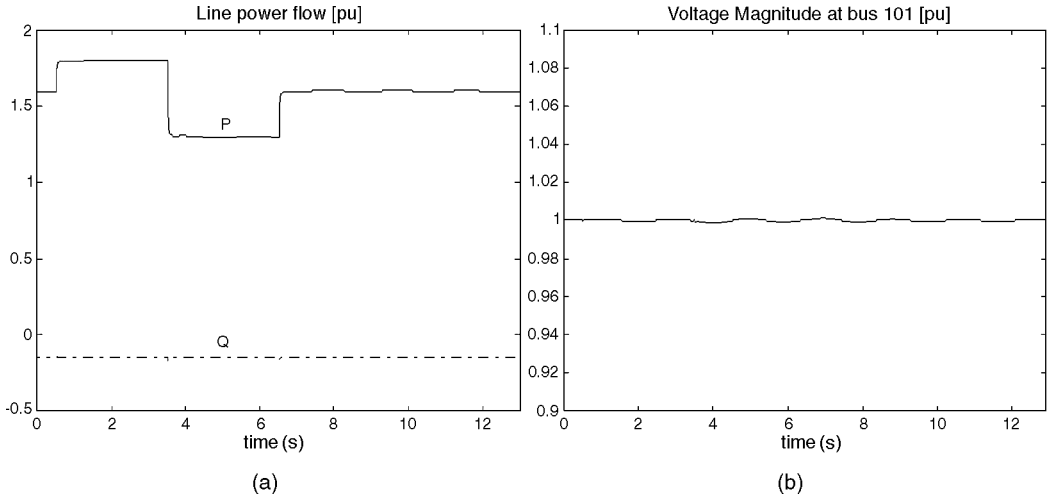

FIGURE 20.22 UPFC changing real power reference (P).

is raised to 1.8 pu and at time 3.5 s it is dropped to 1.3 pu; at time 7.5 s the system returns to the initial operating condition as shown in Fig. 20.22a.

- Keep the real power constant while tracking the step changes in the reactive power (at time 0.5 s reactive power flow reference is changed from –0.15 pu to –0.2 pu; at time 3.5 s reference is set to 0.2 pu; and at time 7.5 s the system returns to the initial operating condition as shown in Fig. 20.23a.

Results depicted in Figs. 20.22 and 20.23 show that the UPFC responds almost instantaneously to changes in real and reactive power flow reference values. For both cases the sending bus voltage is regulated at 1 pu, as shown in Figs. 20.22b and 20.23b. Plots also show that the UPFC is able to control real and reactive power flow independently.

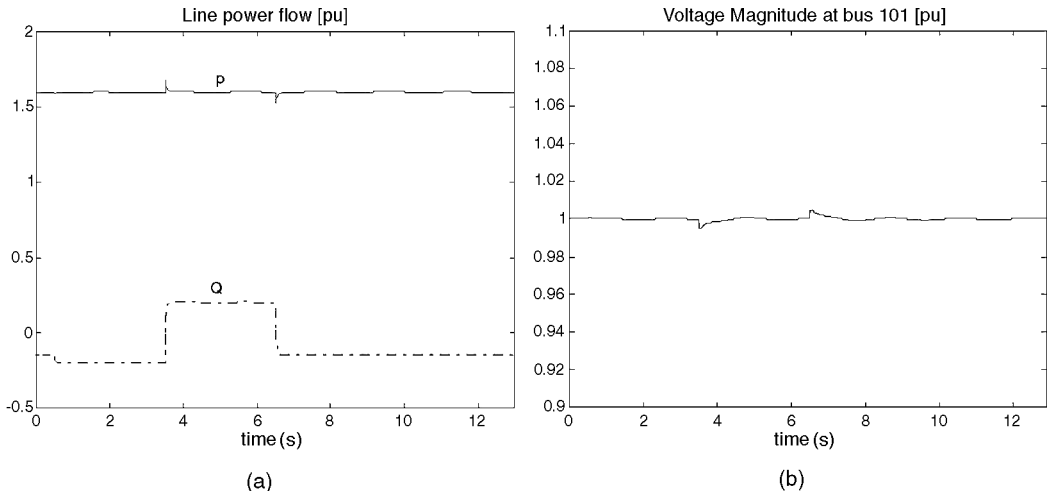

FIGURE 20.23 UPFC changing reactive power reference value (Q).

Operation under Fault Conditions

In this section test system response to a 100-ms three-phase fault applied in area 1, at bus 3, is examined. The fault is cleared by removing one line between the fault bus and bus 101. Two UPFC modes of operation are considered: (1) UPFC operated in the automatic power flow control mode, and (2) UPFC operated in the power oscillation damping control mode.

UPFC Operated in the Automatic Power Flow Control Mode

For comparison reasons, the test system without the UPFC is simulated first. Simulation results for the test system with and without UPFC are shown in Fig. 20.24.

During the steady-state operation each interconnecting tie line carries 197 MW (1.97 pu) from area 1 to area 2. It can be seen from Fig. 20.24a that the line power flow for the test system without the UPFC oscillates long after the fault is cleared, whereas the desired power flow conditions are reached quickly after the fault is cleared for the test system with the UPFC.

For the test system without the UPFC, bus 101 voltage is 0.92 pu, which is below accepted limits. Therefore, the UPFC is operated to keep bus 101 voltage at 1 pu (Fig. 20.24b).

The power angle swings for the test system with UPFC are better damped although it can be seen from Fig. 20.24c that constant power flow has negative effect on the system first swing transient, as reported in Ref. 7.

The DC capacitor voltage fluctuation during the transient is less than 1% of its 22-kV rated value (Fig. 20.24d), which is acceptable for this application.

UPFC Operated in the Power Oscillation Damping Control Mode

To improve the power oscillation damping, the UPFC is operated in the automatic power flow mode but with active damping control. To show the robustness of the proposed control scheme, based on fuzzy logic, discussed earlier, different operating conditions were simulated. The real power that each interconnecting tie-line carries during prefault operating conditions, from area 1 to area 2, is given in Table 20.2.

The fuzzy damping controller is applied to the series converter side. The inputs to the controller are derived from the total real power flow P_t at the UPFC sending bus, as shown in Fig. 20.21. The Max-Product inference engine was used and the centroid defuzzification method was applied. The results obtained with the fuzzy controller are compared with those obtained with the lead-lag controller applied

TABLE 20.2 Operating Conditions (values in MW)

Case	Line 101–13	Line 102–13	Load bus 4	Load bus 14
(a)	232	160	976	1767
(b)	24	160	1176	1567
(c)	143	250	976	1767
(d)	−232	−160	1767	976

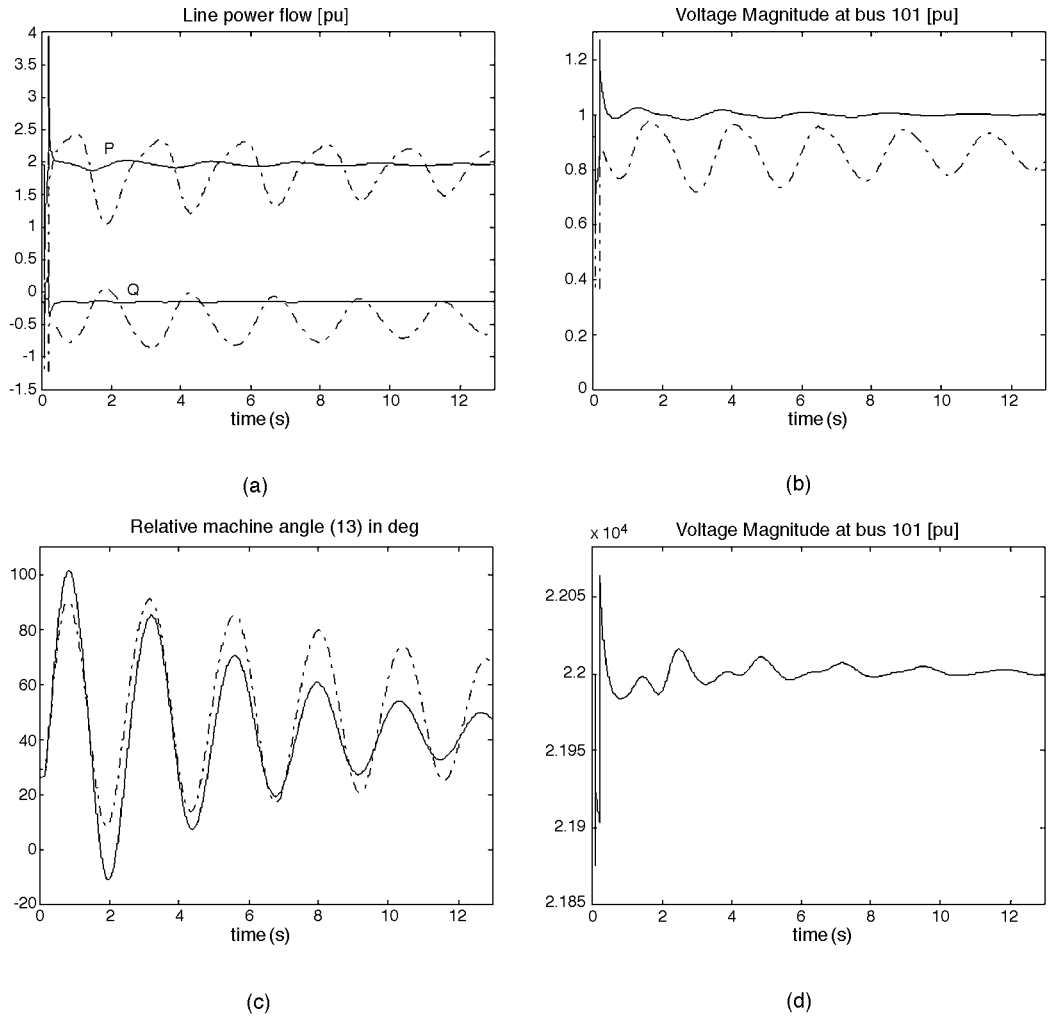

FIGURE 20.24 Simulation results: dashed lines—system without UPFC; solid lines—system with UPFC.

at the shunt converter side. Both fuzzy and lead-lag damping controllers were designed for the first operating condition, (a) in Table 20.2.

Nonlinear simulation results depicted in Fig. 20.25 show that adding a supplementary control signal greatly enhances damping of the generator angle oscillations. It can be seen that the fuzzy damping controller performs better for different operating conditions than the conventional controller.

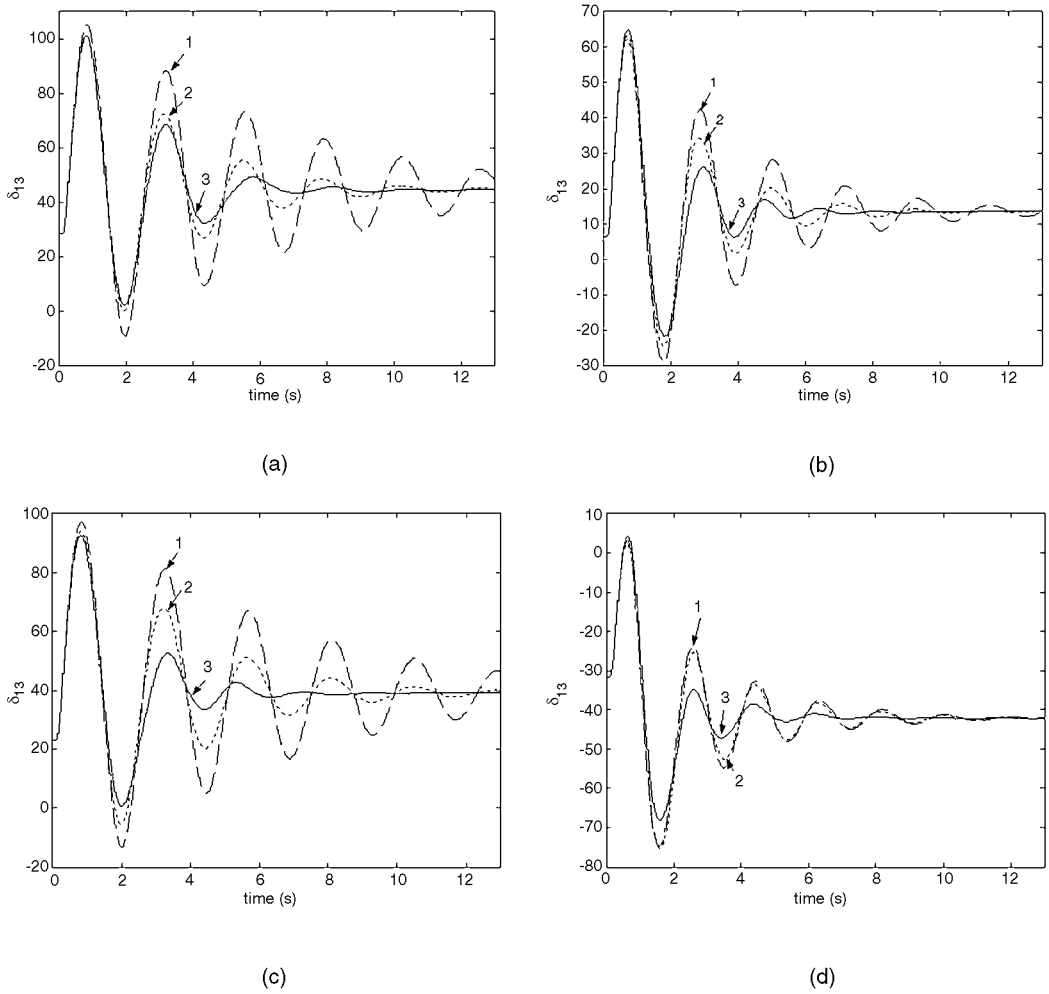

FIGURE 20.25 Relative machine angle δ_{13} in degrees for operating conditions (a to d): 1, without damping controller; 2, lead-lag damping controller; 3, fuzzy damping controller.

20.7 Conclusion

This chapter deals with the FACTS device known as the Unified Power Flow Controller (UPFC). With its unique capability to control simultaneously real and reactive power flows on a transmission line as well as to regulate voltage at the bus where it is connected, this device creates a tremendous impact on power system stability enhancement and loading of transmission lines close to their thermal limits. Thus, the device gives power system operators much needed flexibility to satisfy the demands that the deregulated power system imposes.

Specifically, in this chapter the UPFC is first described and its operation explained. Second, its steady-state and dynamic models, and an algorithm for interfacing it with the power network are presented. Third, basic and damping controller design are developed.

To operate the UPFC in the automatic control mode and to use the UPFC to damp low-frequency oscillations, two controls, basic control and the damping control, are designed. The chapter has shown that the UPFC with its basic controllers is capable of controlling independently real and reactive power flow through the transmission line, under both steady-state and dynamic conditions. Also shown is that the

UPFC can be used for voltage support and for improvement of transient stability of the entire electric power through a supplementary control loop. The proposed supplementary control, based on fuzzy control, is effective in damping power oscillations. The controller requires only a local measurement—the tie-line power flow at the UPFC location. Simulation results have shown that controller exhibits good damping characteristics for different operating conditions and performs better than conventional controllers. The performance is illustrated with a two-area–four-generator test system. Simulation is performed using the MATLAB-based Power System Toolbox package, which is modified to incorporate the UPFC model.

Acknowledgment

The National Science Foundation under Grant ECS-9870041, and the Department of Energy under a DOE/EPSCoR WV State Implementation Award, sponsored some of the research presented in this chapter.

References

1. Dynamic Tutorial and Functions, Power System Toolbox, Version 2.0, Cherry Tree Scientific Software, Ontario, Canada.
2. Mohan, N., Undeland, T. M., and Robbins, W. P., *Power Electronics: Converters, Applications and Design,* 2nd ed., John Wiley & Sons, New York, 1995.
3. Hingorani, N. G. and Gyugyi, L., *Understanding FACTS Devices,* IEEE Press, New York, 2000.
4. Nabavi-Niaki, A. and Iravani, M. R., Steady-state and dynamic models of unified power flow controller (UPFC) for power system studies, *IEEE Trans. Power Syst.,* 11(4), 1937–1943, 1996.
5. Uzunovic, E., Canizares, C. A., and Reeve, J., Fundamental frequency model of unified power flow controller, in *Proceedings of the North American Power Symposium (NAPS),* Cleveland, OH, October 1998.
6. Uzunovic, E., Canizares, C. A., and Reeve, J., EMTP studies of UPFC power oscillation damping, in *Proceedings of the North American Power Symposium (NAPS),* San Luis Obispo, CA, October 1999, 405–410.
7. Huang, Z., Ni, Y., Shen, C. M., Wu, F. F., Chen, S., and Zhang, B., Application of unified power flow controller in interconnected power systems—modeling, interface, control strategy and case study, presented at *IEEE Power Eng. Society Summer Meeting,* 1999.
8. Wang, H. F., Applications of modeling UPFC into multi-machine power systems, *IEE Proc. Generation Transmission Distribution,* 146(3), 306–312, 1999.
9. Jantzen, J., Design of fuzzy controllers, Technical Report No. 98-E 864 (design), Department of Automation, Technical University of Denmark, Lyngby, August 1998.
10. Hsu, Y. Y. and Cheng, C. H, Design of fuzzy power system stabilizers for multimachine power systems, *IEE Proc.,* 137C(3), 233–238, 1990.
11. Hiyama, T., Hubbi, W., and Ortmeyer, T., Fuzzy logic control scheme with variable gain for static Var compensator to enhance power system stability, *IEEE Trans. Power Syst.,* 14(1), 186–191, 1999.
12. Hiyama, T., Fuzzy logic switching of thyristor controlled braking resistor considering coordination with SVC, *IEEE Trans. Power Delivery,* 10(4), 2020–2026, 1995.